Journal of Applied Polymer Science

Thermal Properties and Crystallization Behavior of Bamboo Fiber/High-Density Polyethylene Composites: Nano-TiO_2 Effects

Peng Fei,[1,2] Benhua Fei,[1] Yan Yu,[1] Hanguo Xiong,[2] Jun Tan[2]

[1]International Center for Bamboo and Rattan, Beijing, 100102, People's Republic of China

[2]College of Food Science and Technology, Huazhong Agricultural University, Wuhan, 430070, People's Republic of China

Correspondence to: Y. Yu (E-mail: yuyan9812@icbr.ac.cn) or H. Xiong (E-mail: xionghanguo@163.com)

ABSTRACT: In this study, bamboo fiber/high-density polyethylene (HDPE) composites were prepared, and the effects of nano-TiO_2 on their thermal properties and crystallization behavior were investigated via thermal gravimetric analysis (TGA), differential scanning calorimetry (DSC), X-ray diffraction (XRD), and Fourier transform infrared spectroscopy (FTIR). The results show that the addition of nano-TiO_2 improved the thermal stability and had a dual function in the crystallization behavior of the composites. On one hand, it functioned as a nucleating agent. The addition of 2 wt % nano-TiO_2 promoted the crystallization, which caused the increase of the crystallization rate and crystallinity degree, as well as the micronization of the crystalline grain. On the other hand, intermolecular hydrogen bonds and covalent bonds were formed between nano-TiO_2 and the polymer matrix, which hindered the crystallization of the composites. When the content of nano-TiO_2 was continually increased, the inhibitory effect of the crystallization was gradually enhanced, which resulted in a decrease in the crystallization rate and crystallinity degree of the composites. © 2013 Wiley Periodicals, Inc. J. Appl. Polym. Sci. **2014**, *131*, 39846.

KEYWORDS: biomaterials; fibers; thermoplastics; crystallization

Received 17 April 2013; accepted 13 August 2013

DOI: 10.1002/app.39846

INTRODUCTION

Thermoplastic materials reinforced with natural fibers, replacing glass fibers and other synthetic materials, have attracted much attention in research and industrial fields in recent years.[1–4] Such attention is not only because of environmental concerns, but also of the necessity of providing a high-performance, multi-functional product at a low-cost. Bamboo is an abundant natural resource in Asia and South America, and is gaining worldwide renown as a potential reinforcement for polymer composites because of its innate properties such as low density, high tensile modulus, and low elongation at break.[5] The superior mechanical properties of bamboo are mainly attributed to its unidirectionally oriented fibers, which account for 40% of the culm by volume.[6] Moreover, bamboo only takes several months to grow,[7] whereas wood needs more than 10 years. The reported growth rate of bamboo may seem unbelievable, but the fastest-growing bamboo can vertically grow at a rate of two inches per hour. In particular moso bamboo species, a height of 60 feet can be achieved in just 3 months.[8]

Blending natural fibers with thermoplastic materials is widely considered as an economical technique for producing composites with the desirable combination of specific properties and the ability to be degraded or recycled after the product has served its purpose.[5] However, the low interfacial interactions between hydrophilic natural fibers and hydrophobic thermoplastic matrices may degrade the physical properties of the composites, thereby reducing their potential as reinforcing agents.[9] Many efforts to overcome this situation involve the grafting of compounds onto the fibers by using various coupling agents or bonding agents or the pretreatment of fibers with suitable chemicals.[10–12] Araújo et al.[13] grafted maleic anhydride (MA) and poly (ethylene-*co*-vinyl acetate) (EVA) onto high-density polyethylene, and discovered that MA improved the thermal stability of HDPE/fiber composites more remarkably than EVA. Ismail et al.[14] studied the effects of a silane coupling agent on the mechanical properties and curing characteristics of bamboo fiber/rubber composites. Zhang et al.[5] explored the effects of MA-g-PP additives on the interfacial strength of polypropylene (PP)/polylactic acid (PLA)/bamboo fiber composites.

Inorganic nanoparticles are also used to improve the properties of blended composites. Among all the potential nanocomposite precursors, those based on clay and layered silicates have been studied most extensively probably because the starting clay materials are easily available and their intercalation has been extensively studied.[15] Giannelis[16] used layered silicates as an inorganic phase to enhance the properties of polymer nanocomposites, and he discovered that the addition of small quantities

of inorganic materials that are dispersed at the nanometer level was an effective strategy to overcome the low interfacial interactions between natural fibers and thermoplastic matrices. Vertuccio et al.[17] studied the reinforcement of nanoclay with polycaprolactone (PCL)/starch blends, and they discovered that nanoclays could improve the physical properties of the composites. Nano-TiO_2, which is an inorganic nanoparticle with a large specific surface area and a high surface energy, has been extensively studied in the field of photocatalysis because of its special photochemical property.[18] Nano-TiO_2 has different properties depending on the crystal form. Anatase nano-TiO_2 has been widely employed in the research and development of solar cells,[19] sewage disposal,[20] antibacterial materials,[21] and self-cleaning materials[22] because of its high photocatalytic activity. Rutile nano-TiO_2 has been used in improving the weather resistance of polymer materials as an ultraviolet absorbent.[23] Besides, several —OH groups and dangling bonds were adsorbed on the surface of nano-TiO_2, which may remarkably affect the physical properties of natural fibers/thermoplastic composites.[24] However, relevant studies have seldom been reported.

The physical properties of natural fibers/thermoplastic composites include elastic modulus, tensile strength, stiffness, fracture behavior, drawing behavior, electrical and optical properties, permeability to vapors, and so on. All of these properties are directly related to the crystalline microstructure of the composites. Morphological features such as crystallinity degree, spherulite size, lamella thickness, and crystallite orientation have a profound effect on the final macroscopic properties of the polymer matrix, and consequently, the composite.[25,26] One of the most important factors that affect the properties of polymers is the variation of crystallinity degree.[27] Moreover, crystallization can happen in two different ways: cylindrical crystallization, which is caused by self-nucleation, a kind of homogeneous nucleation that generates β-form crystals from α-form crystals; and transcrystallinity, which is a heterogeneous nucleation that generates α layers from the fiber surface.[13,28] Felix et al.[29] measured the single-fiber fragmentation and found that the presence of transcrystallinity improved the shear transfer between the cellulose fiber and PP matrix.

In this article, bamboo fiber/HDPE/nano-TiO_2 composites were prepared, and the effect of nano-TiO_2 on the thermal properties and crystallization behavior of the composites were investigated.

EXPERIMENT

Materials

Moso bamboo fiber (the length varied from 100 to 150 μm and provided by Research Institute of Comprehensive Utilization of Biomaterials, Huazhong Agricultural University, China) was first dried in 105°C for 48 h. HDPE (5000 s), a product of Daqing Petrochemical with a melt index of 0.7 g/10 min, was used without any treatment. Rutile nano-TiO_2 (40 nm), obtained from Aladdin reagent, Wuhan, China, was dried in vacuum at 105°C for 48 h before use. Absolute ethyl alcohol and poly (ethylene-*co*-vinyl acetate) (EVA) were analytical grade and used as received.

Sample Preparation

Preparation of Bamboo Fiber/HDPE Composite. Bamboo fiber (50 g), HDPE (50 g), and EVA (10 g) were poured into a JB200-D electromotion stirrer (Shanghai specimen and model factory, China) and stirred at high-speed (>1000 rpm) at a constant temperature for 20 min for complete mixing. The resulting mixture was then thoroughly kneaded in a kneading machine for about 1 h. Finally, the composites were compress-molded at 180°C into 2-mm thick sheets at a pressure of 25 MPa for 5 min by using a hot press R-3202 (Wuhan Qien science & Technology development), and was coded as BHN0.

Preparation of Bamboo Fiber/HDPE/Nano-TiO_2 Composites. Different amounts of nano-TiO_2 (2, 4, 6, and 8 g) were added to a beaker with corresponding volumes of absolute ethyl alcohol (150, 300, 450, and 600 mL, respectively), and dispersed at 600 W for 30 min by using an Ultrasonic Processor FDL-1200 (intermittent dispersion of pulsing on for 1 s and off for 2s, with a frequency of 20 kHz). Bamboo fiber (50 g), HDPE (50 g) and EVA (10 g) were then added to solution, which was then stirred using a motor stirrer at high-speed (>1000 rpm) at 90°C until the alcohol completely evaporated. The mixture was then poured into a kneading machine and thoroughly kneaded for 1 h. Finally, the composite was compressed into 2-mm thick sheets in the same conditions used to prepare the bamboo fiber/HDPE composites. The composites with different nano-TiO_2 contents were coded as BHN1, BHN2, BHN3, and BHN4. The bamboo fiber/HDPE composite without nano-TiO_2 was coded as BHN0.

Characterizations

The surfaces and morphologies of bamboo fiber/HDPE composites were investigated by a Hitachi (Japan) S-4800 field emission scanning electron microscope (FESEM). The surfaces were sputter coated with gold prior to examination. The FTIR spectra were recorded with a Nicolet (USA) Nexus 470 FTIR spectrometer. The powdered samples were blended with potassium bromide (1:100) and laminated. The wave range, from 4000 to 400 cm^{-1}, was scanned 32 times for spectrum integration, and the scanning resolution was 4 cm^{-1}. The samples of 5–7 mg used for the thermogravimetric analysis were dried in an oven for 3 h at 100°C. The TGA equipment (TA2900 from TA Instruments) was programmed for heating from 20 to 600°C with a heating rate of 10°C min^{-1} under nitrogen atmosphere. The thermal properties of the composite were performed by using a DSC 200PC (NETZSCH, Germany) under nitrogen atmosphere. The samples of 5–10 mg were encapsulated into aluminum pans and were heated from 20 to 200°C at a rate of 10°C min^{-1}, and then the temperature was kept at 200°C for 10 min to erase previous thermal history of melt characterization. Subsequently samples were cooled to 10°C at the rate of 10°C min^{-1} to obtain the crystallization curve and kept at this temperature for 10 min; after then, the samples were heated to 200°C at the rate of 10°C min^{-1} to obtain the melting curve. During the process, dry nitrogen was purged into the DSC cell with a flow rate of 60 mL min^{-1} to prevent thermal degradation. There was no change in sample weights after the completion of the all thermal analysis process. X-ray diffraction (XRD) measurements were performed on the sample composites by

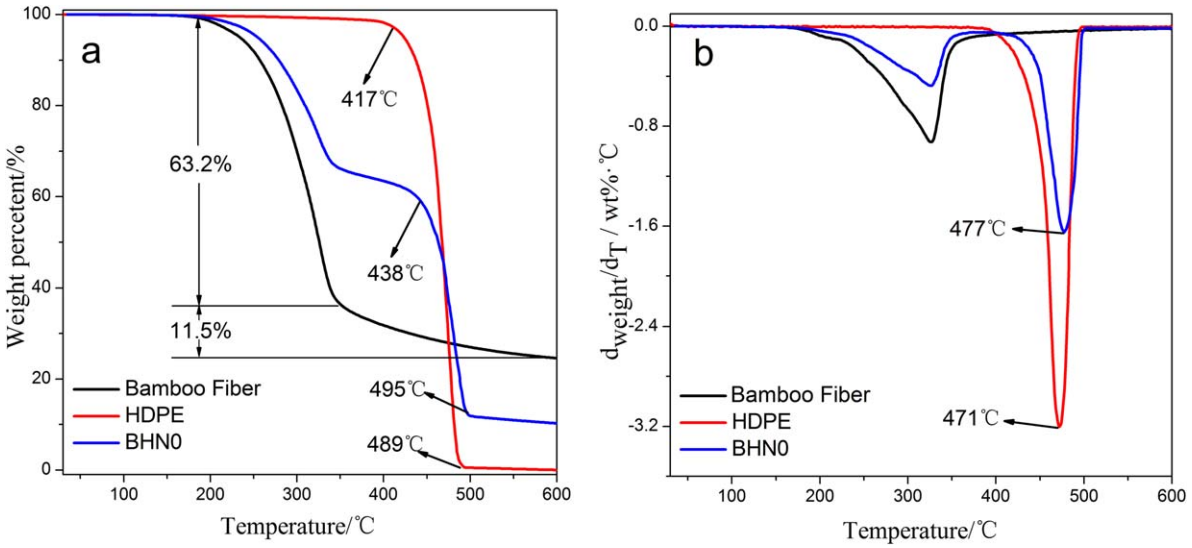

Figure 1. TG curves of pure HDPE, bamboo fiber, and BHN0 composite (a) and the first derivative curves of the same samples (b). BHN0: nano-TiO_2 content was 0 wt %. [Color figure can be viewed in the online issue, which is available at wileyonlinelibrary.com.]

means of a Rigaku (Japan) D/max-RB X-ray diffractometer, and a Cu Kα target was used at 40 kV and 50 mA. The diffraction angle ranged from 60° to 5°.

RESULTS AND DISCUSSION

Thermogravimetric Analysis

Figure 1(a) shows the thermogravimetric (TG) curves of HDPE, bamboo fiber, and their blend composite at a heating rate of 10°C min^{-1} in an N_2 atmosphere. Figure 1(b) shows their respective derivative thermograms (DTG). From the TG curves, HDPE exhibits only one degradation peak, whereas bamboo fiber has two. The first weight loss process of the bamboo fiber ranging from 180 to 349°C is attributed to the thermal degradations of pectin, lignin, and hemicellulose. The second weight loss is associated with the decomposition of the α-cellulose present in the fiber.[30] The second weight loss (11.5%) is much lower than the first one (63.2%), which is attributed to the high stability of α-cellulose. For the blend composites, bamboo fiber decomposes during the whole process, whereas HDPE starts to decompose at 438°C with the maximum weight loss rate at 477°C. The TG curve of HDPE shows the start of volatile emission at 417°C [Figure 1(a)] with the maximum weight loss rate at 471°C [Figure 1(b)], which are 21 and 6°C, lower than that of HDPE in the blend composites, respectively. This result may be caused by the intertwining of the cellulose chain with the HDPE molecule, which hampered the decomposition of HDPE. This result can be further confirmed based on the ending temperature of the volatiles at 489°C for pure HDPE, which is 6°C lower than that of HDPE in the blend composites.

Figure 2 shows the TG curves of BHN composites (all curves were corrected by deducting nano-TiO_2 weight). As shown in Figure 2(a), the nanocomposites exhibited a higher thermal stability than the blend. The thermal stability of the nanocomponents follows the sequence BHN3>BHN2>BHN4>BHN1>BHN0. The enhancement in the thermal stability of the composites by nano-TiO_2 may be attributed to several factors. On one hand, nano-TiO_2 could be easily dispersed into the macromolecular chains of the composites, which reduced the free volume in the micro-zone and strengthens the molecular chain rigidity. As a result, the polymer segmental motion of the composites was restricted, and the fracture energy of the molecular chains increased. On the other hand, TiO_2 was a kind of semiconductor material, a Ti atom was connected to other Ti atoms via bridging oxygen atoms and the total chemical composition was denoted TiO_2. As seen in Figure 3, this structure left plentiful dangling bonds (unpaired electrons) on surface Ti or O atoms due to the small-size of nano-TiO_2. These dangling bonds could interact with polymer molecules and enhanced the crosslinking of the composites. The enhancement in the crosslinking also restricted the molecular motion and ionic mobility, which contributed to the increase in thermal stability. In particular cases when chemical bonding was formed and associated with intermolecular forces between nanoparticles and composites, the thermal stability of the composites would be evidently enhanced.[31] The enhancement in thermal stability increased with increasing nano-TiO_2 content, but was slightly reduced when the content reached 8 wt %. This behavior probably occurred because the surface interactions of nano-TiO_2 led to nanoparticle agglomeration when the amount of nanoparticles was too high. Thus, the compatibility between the nanoparticles and polymer matrix was poor, which decreased thermal stability.

The weight percentage of char residues is presented in Figure 2(b) to verify the effect of nano-TiO_2 on the thermal stability of BHN composites. The formation of char was mainly associated with the bamboo fiber because pure bamboo fiber produced 24.9% char residues, whereas HDPE only produced 0.3%. When the nano-TiO_2 content was increased from 0 to 6%, the char residues of the composites increased from 10.5 to 15.2%. The thermal stability enhancement was recognized to be a consequence of the dispersion of nano-TiO_2 as well as the interaction between the nano-TiO_2 and bamboo fiber/HDPE, which led to

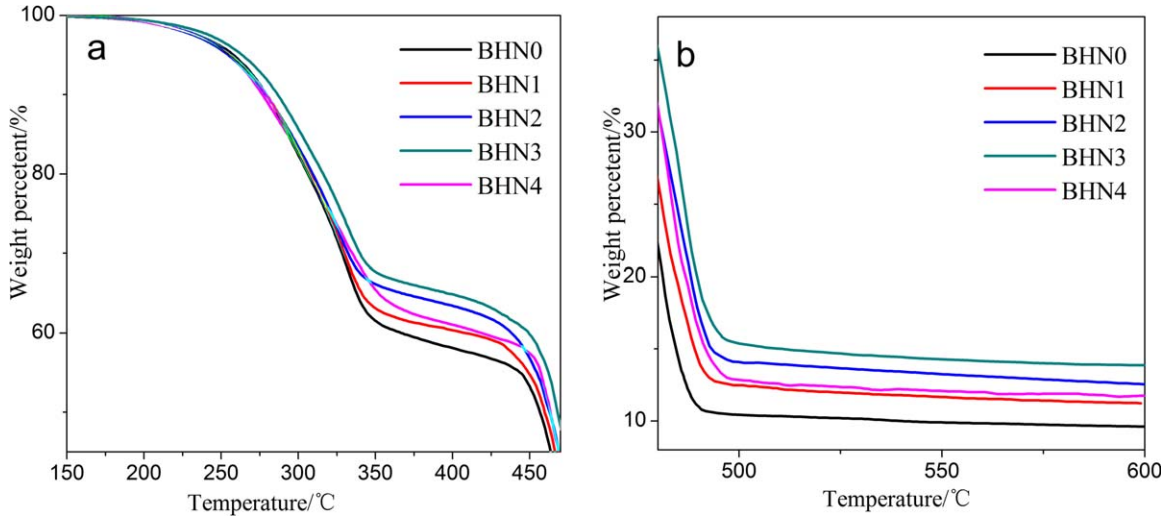

Figure 2. TG curves of different BHN composites. BHN0, BHN1, BHN2, BHN3, BHN4 correspond to increasing nano-TiO_2 contents from 0 to 8 wt %. All curves were corrected by deducting the nano-TiO_2 weight. [Color figure can be viewed in the online issue, which is available at wileyonlinelibrary.com.]

a decrease in heat permeability and ionic mobility in the blend matrix during the heating scans.

Morphology of the Composites

The morphology of bamboo fiber/HDPE composites was characterized by FESEM (Figure 4). It could be clearly seen that, compared with that of the composite without nano-TiO_2, the surface morphology of the composites contained nano-TiO_2 exhibited much more homogeneous and smooth [Figure 4(a,b)]. It suggested that the addition of nano-TiO_2 greatly improved the miscibility and compatibility between bamboo fibers and HDPE. The cross section images of BHN composites [Figure 4(c,d)] present the same result. This was because the dangling bonds absorbed on the surfaces of nano-TiO_2 interacted with bamboo fiber and HDPE and formed intermolecular interactions between the two polymers, and further enhanced the compatibility of the BHN composites.

DSC Analysis

The differential scanning calorimetry (DSC) curves of the BHN composites are shown in Figures 5 and 6. Comparing the three steps in Figures 5(a,b) and 6(a), an endothermic event for bamboo fiber is only observable in the first heating step [Figure 5(a)], which may be because some crystalline domains in the cellulose of the natural fiber do not have conditions of crystallization in the cooling step [Figure 6(a)].

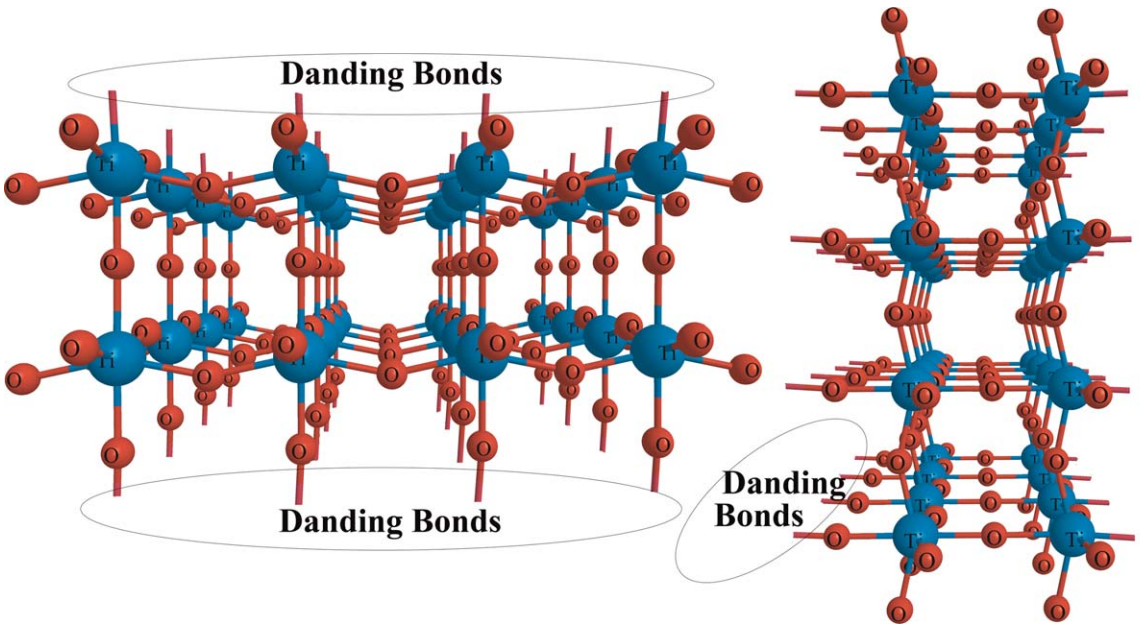

Figure 3. Molecular structure and dangling bonds of nano-TiO_2. [Color figure can be viewed in the online issue, which is available at wileyonlinelibrary.com.]

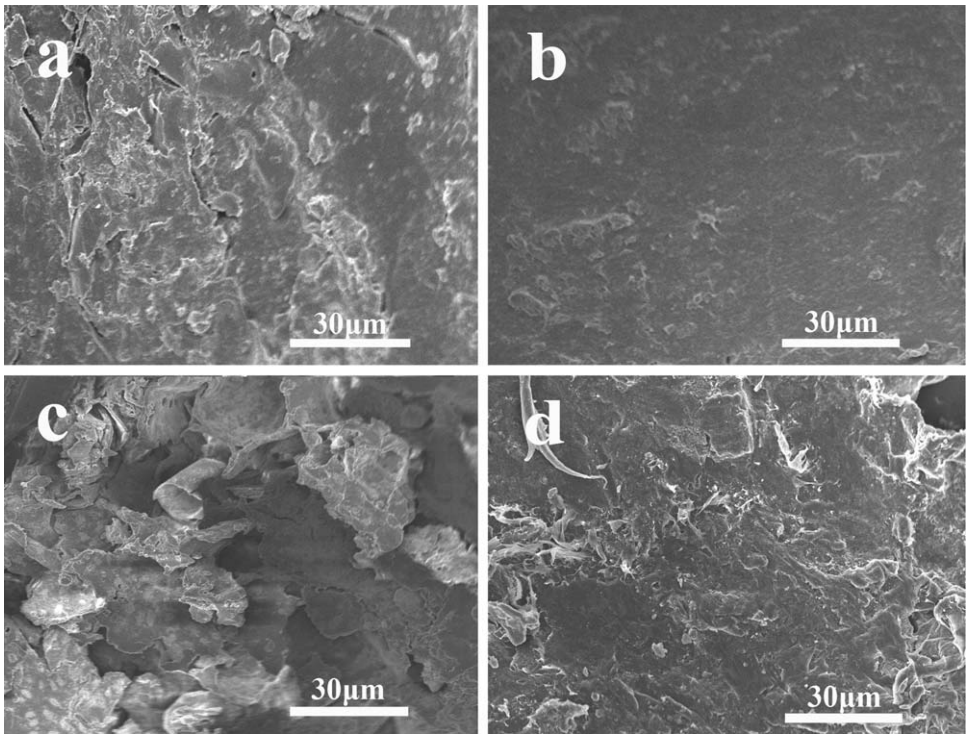

Figure 4. FESEM micrographs of the surfaces and cross sections of BHN composites. (a) Surface of the BHN composite without nano-TiO_2; (b) Cross section of the composite contained nano-TiO_2; (c) Surface of the BHN composite without nano-TiO2; (d) Cross section of the BHN composite contained nano-TiO_2.

From the DSC curve of Figure 5(b) (the first heating step, and the cooling step was performed to erase the previous thermal history of melt characterization), the crystallinity values for the HDPE component in the composites were determined based on the melting peak area by using the following equation:

$$X_C = \frac{\Delta H_m}{\varphi \Delta H_m^0} \times 100\% \quad (1)$$

where ΔH_m is the enthalpy of fusion of the sample, ΔH_m^0 is the heat of fusion for 100% crystalline HDPE (taken to be 293 J g^{-1}[32]), and φ is the weight fraction of HDPE in the composites.

The crystallinity degree of the HDPE component in the BHN0 composite decreased by about 13.8% compared with pure HDPE [Figure 5(b), inset]. This decrease happened because the fiber chains were inserted into the molecular structure of HDPE and were intertwined with the HDPE molecule, which disturbed the nucleation and the local arrangement of the HDPE molecular chains during the cooling crystallization process.

The crystallinity degree of the HDPE component in the composites increased with the addition of 2 wt % nano-TiO_2. One explanation is that nano-TiO_2 contributed in promoting the crystallization as a nucleating agent because of its small size and large specific surface area. In general, HDPE with a symmetric and simple structure can easily nucleate during crystallization, which can hardly be affected by any nucleating agent. However, in this case, the addition of bamboo fiber bounded the molecular chains of HDPE and hindered the nucleation.

When the contents of nano-TiO_2 were continuously increased, the crystallinity degree of HDPE decreased. This phenomenon probably occurred because nano-TiO_2 had a dual effect on crystallization, namely, as promoter and as a hindrance. Because of the plentiful dangling bonds absorbed on the surface atoms, nano-TiO_2 could be easily dispersed into the macromolecular chains and formed intermolecular interactions with cellulose and HDPE, which disturbed the parallel direction of the cellulose/HDPE chains. On the other hand, the addition of nano-TiO_2 increased the rigidity of cellulose/HDPE chains, which also hindered the crystallization and resulted in a decrease in the crystallinity of the composite. With every increase in the amount of nano-TiO_2, the promotion effect of nano-TiO_2 as a nucleating agent was maintained or slightly increased, whereas the inhibitory effect was enhanced by a large margin. Thus, the crystallinity degree of the composites decreased. The crystallinity degree slightly increased when the nano-TiO_2 content was increased to 8%. This increase may be attributed to the agglomeration of excess nanoparticles.

Crystallinity versus time for crystallization of BHN composites during the cooling crystallization process is plotted in Figure 6(b). The crystallization time of the composites was determined using the following equation:

$$t = (T_0 - T)/\upsilon \quad (2)$$

where T_0 is the initial crystallization temperature, T is crystallization temperature, and υ is cooling rate.

Based on Figure 6(b), the half-crystallization time of BHN0 composite was 0.616 min, which is 21.1% longer than that of pure HDPE. This result verified the inhibitory effects of bamboo fiber on the crystallization of the composites. On the other

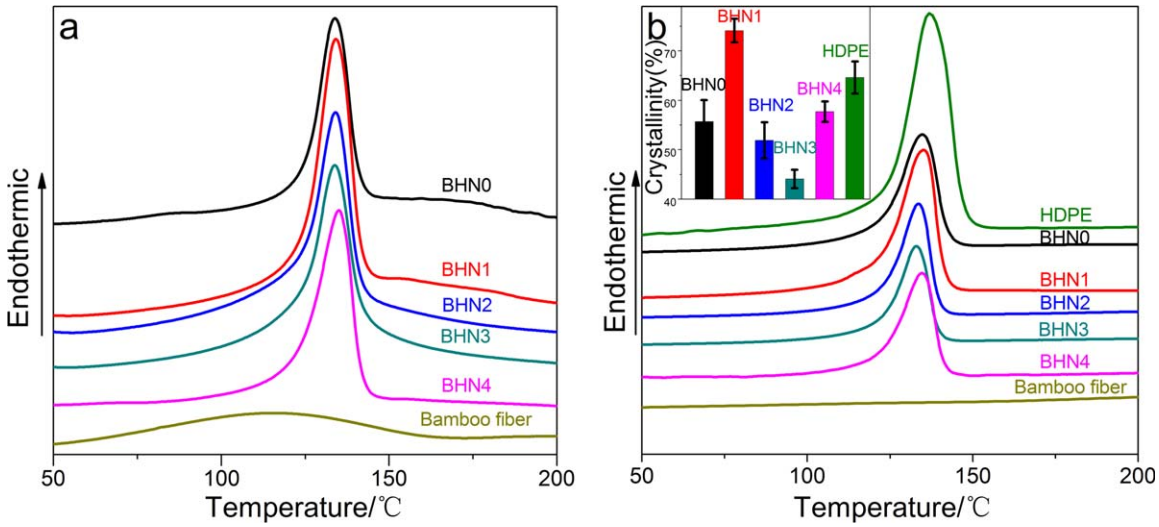

Figure 5. DSC curves and the crystallinity degree of bamboo fiber, HDPE, and BHN composites; (a) the first heating step; (b) second heating step. [Color figure can be viewed in the online issue, which is available at wileyonlinelibrary.com.]

hand, the half-crystallization time of BHN1 was 0.513 min, which is 16.7% shorter than that of BHN0 composite. This result confirmed that nano-TiO_2 contributed in promoting crystallization. Moreover, the half-crystallization time of BHN2 was 0.552 min, which is 6.7% shorter than that of BHN1. This result verified the inhibitory effects of nano-TiO_2 on crystallization.

XRD Analysis

An X-ray diffraction (XRD) study was carried out to investigate the crystallization behavior of bamboo fiber, HDPE, and bamboo fiber/HDPE polyblends. The XRD spectra of HDPE and BHN0 composite are presented in Figure 7. The pure HDPE diffraction peaks of crystal plane (110) and (200) are strong and sharp, which indicates a big and unbroken crystalline grain. However, the diffraction intensity drastically decreased during the blending with bamboo fiber. This phenomenon confirmed that the fiber chains were intertwined with the HDPE molecular chains and further damaged its crystal structure.

The crystallinity degree of the composites was calculated based on the crystalline and noncrystalline areas using the following equation:

$$X_c = \frac{F_c}{F_c + F_a} \times 100\% \quad (3)$$

where F_c is the crystalline area and F_a is the noncrystalline area. The results are shown in Figure 9(a). BHN1 had the highest crystallinity degree at 61.63%, whereas BHN4 had the lowest at 45.45%. This variation trend is in agreement to that derived from DSC. The difference between the values derived from the

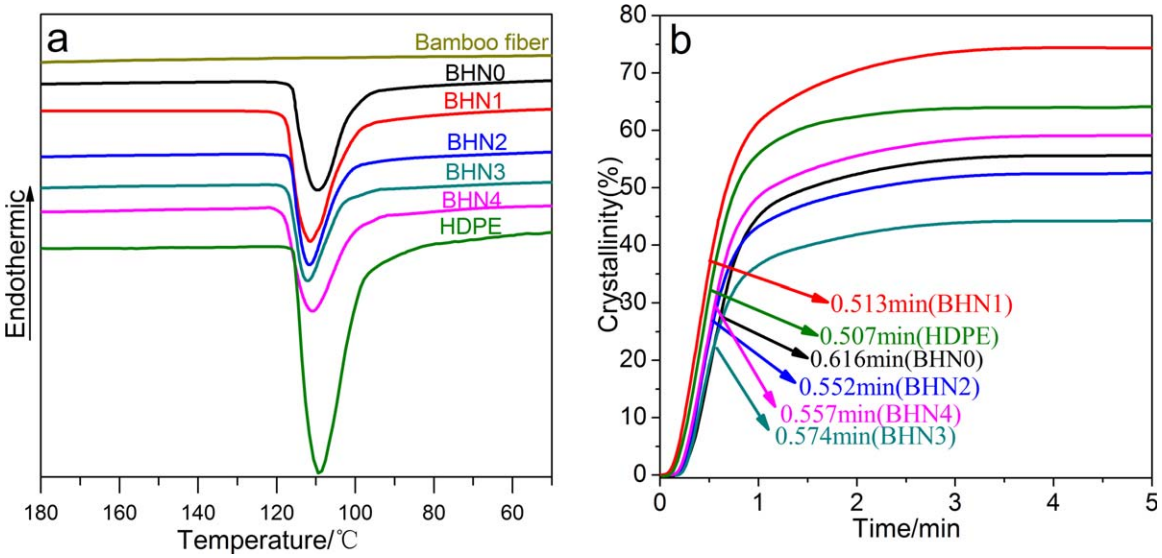

Figure 6. DSC curves and plots of X_c versus time for the crystallization of bamboo fiber, HDPE, and BHN composites; (a) the cooling step; (b) plots of crystallinity versus time during crystallization. [Color figure can be viewed in the online issue, which is available at wileyonlinelibrary.com.]

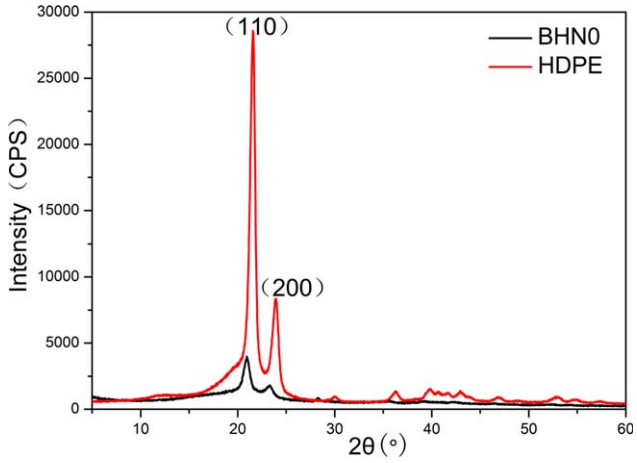

Figure 7. XRD patterns of the BHN0 composite and HDPE. [Color figure can be viewed in the online issue, which is available at wileyonlinelibrary.com.]

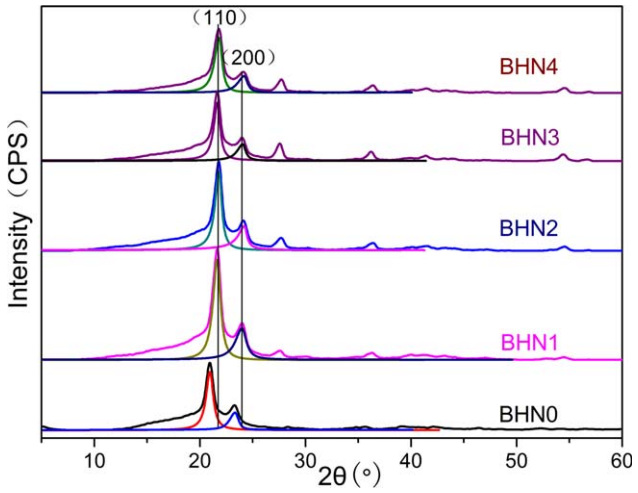

Figure 8. XRD patterns of the BHN composites. [Color figure can be viewed in the online issue, which is available at wileyonlinelibrary.com.]

two methods mainly caused by the entirely different measuring principle of the two methods and the indefinite boundary between the crystalline and noncrystalline regions.

The XRD patterns of the BHN composite in a 2θ range of 5°–60° are shown in Figure 8. A peak-fitting program was used to determine the crystalline formed in the samples.[33] The diffraction peaks at about 27.7°, 36.2°, and 54.5° are attributed to the characteristic diffraction peaks of rutile nano-TiO_2.[34] Figure 8 also shows that the 110 and 200 diffraction peaks of the composites at 2θ of about 21° and 23°, respectively, shifted to a larger angle direction when nano-TiO_2 was added. The change in diffraction peak angle indicates the distortion of the HDPE lattice because nano-TiO_2 was dispersed into the macromolecular chains and entered into the lattice of the HDPE component. Thus, the crystal morphology changed.

To analyze further the effects of nano-TiO_2 on the crystalline behavior of the composites, the crystal size of the composites was calculated based on Scherrer equation as follows:

$$D = K\,\lambda / B\cos\theta \tag{4}$$

where D represents the average thickness of crystalline grain, which is vertical to the direction of the crystal face; K is Scherrer constant (taken to be 0.89); λ is the wavelength of the X-ray (for Cu target, taken to be 1.54×10^{-10}m); B is the half-height width of diffraction peak; and θ is the Bragg angle in degrees.

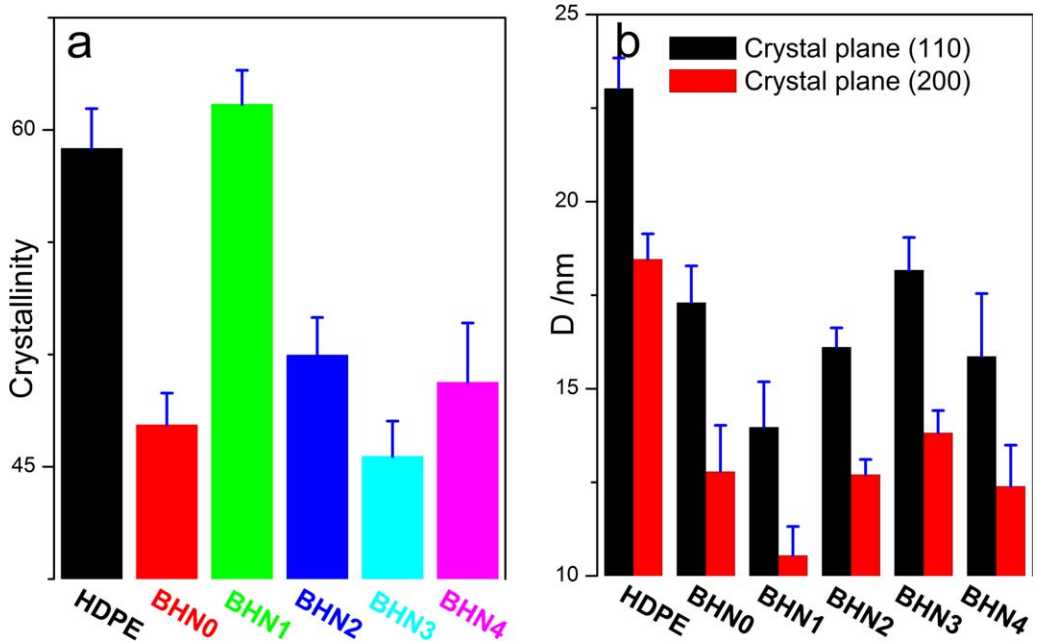

Figure 9. The crystallinity degree and crystal size of HDPE and the BHN composites: (a) The crystallinity of HDPE and the BHN composites; (b) The crystal size of HDPE and the BHN composites. [Color figure can be viewed in the online issue, which is available at wileyonlinelibrary.com.]

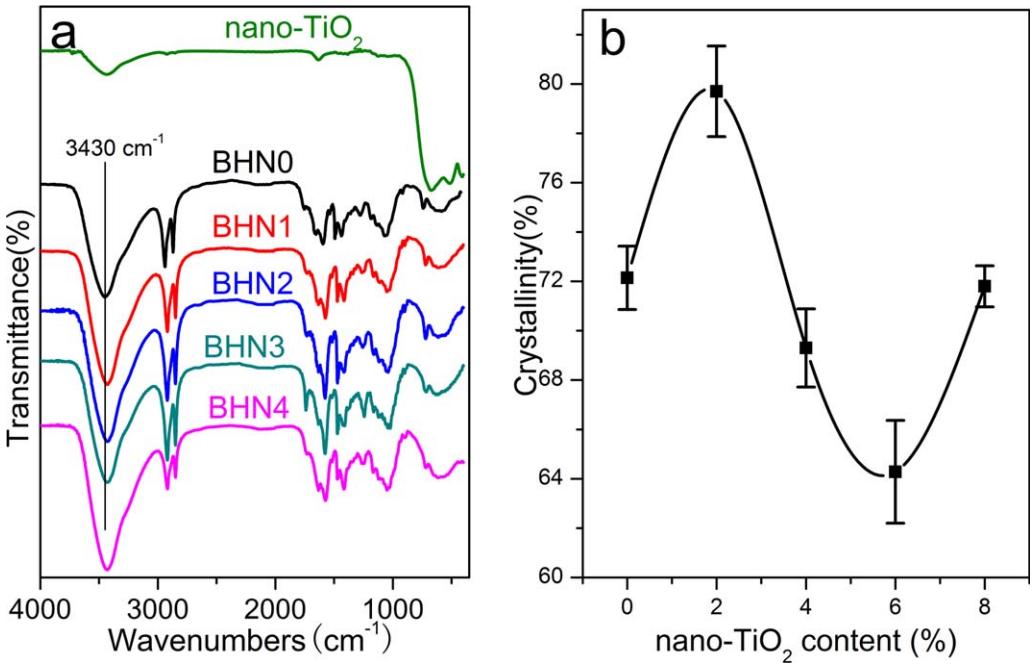

Figure 10. FTIR spectra and crystallinity of nano-TiO_2 and BHN composites: (a) FTIR spectra of nano-TiO_2 and BHN composites; (b) Crystallinity of BHN composites. [Color figure can be viewed in the online issue, which is available at wileyonlinelibrary.com.]

The calculated crystal sizes of the composites are shown in Figure 9(b). The crystal size decreased when blended with bamboo fiber because of the hinderding effect of the bamboo fiber on the rearrangement and crystallization of the HDPE molecular chains. The crystal size decreased when 2 wt % nano-TiO_2 was added. Thus, nano-TiO_2 functioned as a nucleating agent, which resulted in heteronuclear crystallization. Such involvement led to the micronization of the crystalline grain and the increase in crystallinity degree.[35] This result was in agreement to the speculation of nano-TiO_2's function as a nucleating agent based on DSC results. When the contents of nano-TiO_2 were continuously increased, the crystallinity degree decreased and the crystal size increased because the crosslinking of nano-TiO_2 was gradually enhanced with increasing nano-TiO_2 content. The improvement of the interpenetrating network structure by combining nano-TiO_2 with bamboo fiber/HDPE not only inhibited the growth of crystalline by restricting the molecular motion and rearrangement, but also decreased the quantity of crystallization center during the cooling crystallization process.[36] Thus, the nucleating agent function of nano-TiO_2 were weaken. In a microscopic view, the crystal size of the composites increased with increasing nano-TiO_2 content, whereas in a macroscopic view, the crystallinity degree decreased.

FTIR Analysis

The effects of nano-TiO_2 on the crystallization behavior and molecular structure of the bamboo fiber/HDPE composites were studied via Fourier transform infrared (FTIR) spectroscopy.

Zerbi et al.[37] revealed that the crystallinity of HDPE can be determined by the empirical relation

$$X_c = 100 - \frac{1 - \frac{I_a/I_b}{1.233}}{1 + I_a/I_b} \times 100 \quad (5)$$

where X_c represents the percentage of the crystalline content and the constant 1.233 represents the relation of intensities of these bands of a totally crystalline HDPE. I_a and I_b can be derived from the bands at either 1474 and 1464 cm^{-1} or 731 and 718 cm^{-1}, respectively. The doublet peaks corresponded to polyethylene crystalline content (1474 and 731 cm^{-1}) and amorphous content (1464 and 718 cm^{-1}). Colom et al.[2] demonstrated that cellulose fibers show a characteristically intense band at 1430 cm^{-1}, which is assigned to the vibration of the —CH_2 group. The band interacts with that of —CH_2 in HDPE, thereby leading to unreliable results. In our work, crystallinity was calculated using the doublet peaks at 731 and 718 cm^{-1}, and the crystallinity values are shown in Figure 10(b). The crystallinity degree results are in agreement to those obtained from DSC and XRD.

The FTIR spectrum of nano-TiO_2 is shown in Figure 10(a). The absorption peaks at 656, 532, and 412 cm^{-1} were attributed to the characteristic peaks of nano-TiO_2, which was caused by the stretching vibrations and flexural vibration of O—Ti—O. The absorption peaks at around 1634 cm^{-1} and the broad peaks at around 3430 cm^{-1} were assigned to the flexural vibration of H—O—H bonds of the physisorbed water and surface Ti—OH bonds and hydrogen bonded molecular water species respectively.[38] This result implied that plentiful —OH groups were absorbed on the surface of nano-TiO_2, which could form hydrogen bonds with the bamboo fiber. Compared with that of BHN0, the bands at around 3430 cm^{-1} of composites contained nano-TiO_2 shifted to a lower wavenumber. The red shift of the bands confirmed the formation of intermolecular hydrogen

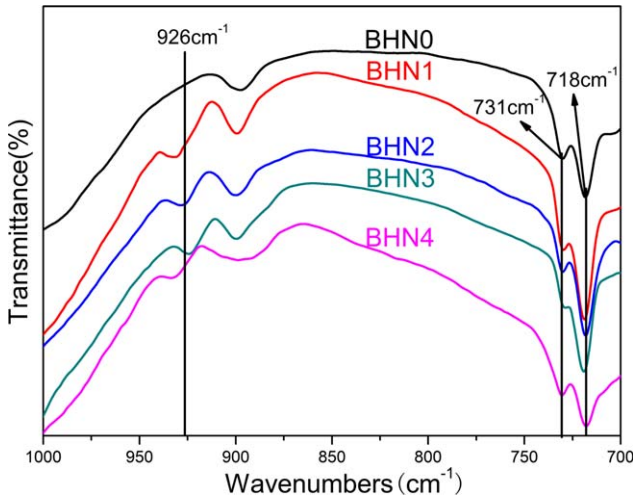

Figure 11. FTIR spectra of BHN composites. [Color figure can be viewed in the online issue, which is available at wileyonlinelibrary.com.]

bonds between bamboo fiber and nano-TiO_2. Aside from —OH, the dangling bonds could also form covalent interactions with bamboo fiber/HDPE. Figure 11 shows the FTIR spectra of the composites at 1000–700 cm^{-1}. BHN0 did not exhibit any peak at 926 cm^{-1}, but BHN1, BHN2, BHN3, and BHN4 exhibited a peak at that position, which may be attributed to the formation of the C—O—Ti group between nano-TiO_2 and bamboo fiber or nano-TiO_2 and HDPE. The presence of the C—O—Ti group and the hydrogen bond improved the interfacial interaction of the composites, the crosslinking extent, and the rigidity of molecular links. These improvements restricted the molecular motion and rearrangement, thereby preventing the nucleation effect of nano-TiO_2 and causing a decrease in the crystallinity degree with increasing nano-TiO_2 content. These findings confirmed the deduction derived from DSC and XRD analyses results. The peak at about 926 cm^{-1} had a significant blue shift, which attributed the agglomeration of excess nanoparticles.

CONCLUSION

The effects of nano-TiO_2 on the thermal properties and crystallization behavior of bamboo fiber/HDPE composites were investigated via TGA, DSC, XRD, and FTIR. The results demonstrate that the addition of nano-TiO_2 enhanced the thermal stability of bamboo fiber/HDPE composites and had a dual function in the crystallization behavior of the composites. On one hand, as a nucleating agent, the crystallization rate and crystallinity degree of the composites increased with the addition of nano-TiO_2, and the crystal morphology was changed. On the other hand, plentiful —OH and unsaturated dandling bonds are adsorbed on the surfaces of nano-TiO_2, which can form hydrogen bonds and covalent bonds between nano-TiO_2 and the polymer matrix and hindered the crystallization of the composites. The inhibitory effect was gradually enhanced with increasing nano-TiO_2 content, which resulted in the decrease of the crystallization rate of composites and crystallinity degree. The influence of nano-TiO_2 on the change in thermal stability could also be related to intermolecular hydrogen bonds and covalent bonds. Moreover, the results also imply that excess nanoparticles would agglomerate when the nano-TiO_2 content reached 8 wt %.

ACKNOWLEDGMENTS

The authors gratefully acknowledge the financial assistance supported by the National Science and Technology Support Program (No. 2012BAD54G01), the Fundamental Research Funds for the Central Universities (No. 2011PY152), and the Huazhong Agricultural University Scientific & Technological Self-innovation Foundation (No. 2012SC21).

REFERENCES

1. Wambua, P.; Ivens, J.; Verpoest, I. *Compos. Sci. Technol.* **2003**, *63*, 1259.
2. Colom, X.; CaÑavate, J.; Pagés, P.; Saurina, J.; Carrasco, F. *J. Reinf. Plast. Comp.* **2000**, *19*, 818.
3. Araujo, J. R.; Mano, B.; Teixeira, G. M.; Spinacé, M. A. S.; De Paoli, M. A. *Compos. Sci. Technol.* **2003**, *63*, 1259.
4. Li, W.; Li, X. Y.; Chen, Y.; Li, X. X.; Deng, H. B.; Wang, T.; Huang, R.; Fan, G. *Carbohydr. Polym.* **2013**, *92*, 2232.
5. Zhang, Y. C.; Wu, H. Y.; Qiu, Y. P. *Bioresource. Technol.* **2010**, *101*, 7944.
6. Zou, L. H.; Jin, H.; Lu, W. Y.; Li, X. D. *Mater. Sci. Eng. C Biol. S.* **2009**, *29*, 1375.
7. Okubo, K.; Fujii, T.; Yamamoto, Y. *Compos. A Appl. S.* **2004**, *35*, 377.
8. Abdul Khalil, H. P. S.; Bhat, I. U. H.; Jawaid, M.; Zaidon, A.; Hermawan, D.; Hadi, Y. S. *Mater. Des.* **2012**, *42*, 353.
9. Fuentes, C. A.; Tran, L. Q. N.; Van Hellemont, M.; Janssens, V.; Dupont-Gillain, C.; Van Vuure, A. W.; Verpoest, I. *Colloid. Surf. A.* **2013**, *418*, 7.
10. Xin, S. J.; Li, X. Y.; Zhu, Y.; Zhang, T.; Lei, Z. J.; Li, W.; Zhou, X.; Deng, H. B. *Colloid Surf. B* **2013**, *105*, 137.
11. Spencer, M. W.; Cui, L. L.; Yoo, Y. J.; Paul, D. R. *Polymer* **2010**, *51*, 1056.
12. Xu, R. F.; Xin, S. J.; Zhou, X.; Li, W.; Cao, F.; Feng, X. Y.; Deng, H. B. *Int. J. Pharm.* **2013**, *438*, 258.
13. Araújo, J. R.; Waldman, W. R.; De Paoli, M. A. *Polym. Degrad. Stabil.* **2008**, *93*, 1770.
14. Ismail, H.; Shuhelmy, S.; Edyham, M. R. *Eur. Polym. J.* **2002**, *38*, 39.
15. Alexandre, M.; Dubois, P. *Mater. Sci. Eng. R.* **2000**, *28*, 1.
16. Giannelis, E. P. *Adv. Mater.* **1996**, *8*, 29.
17. Vertuccio, L.; Gorrasi, G.; Sorrentino, A.; Vittoria, V. *Carbohydr. Polym.* **2009**, *75*, 172.
18. Nakata, K.; Fujishima, A. *J. Photoch. Photobio. C.* **2012**, *13*, 169.
19. Melhem, H.; Simon, P.; Wang, J.; Bin, C. D.; Ratier, B.; Leconte, Y.; Herlin-Boime, N.; Makowska-Janusik, M.; Kassiba, A.; Bouclé, J. *Sol. Energ. Mater. Sol. C.* Available at: http://dx.doi.org/10.1016/j.solmat.2012.08.017.
20. Zhang, F. S.; Nriagu, J. O.; Itoh, H. *J. Photoch. Photobio. A.* **2004**, *167*, 223.

21. Zhang, L.; Bai, X.; Tian, H.; Zhong, L. L.; Ma, C. L.; Zhou, Y. Z.; Chen, S. L.; Li, D. L. *Carbohydr. Polym.* **2011**, *89*, 1060.
22. Li, F.; Li, Q. M.; Kim, H. *Appl. Surf. Sci.* **2013**, *276*, 390.
23. Seentrakoon, B.; Junhasavasdikul, B.; Chavasiri, W. *Polym. Degrad. Stabil.* **2013**, *98*, 566.
24. Fujishima, A.; Zhang, X. T.; Tryk, D. A. *Surf. Sci. Rep.* **2008**, *63*, 515.
25. Kwei, T. K.; Schonhorn, H.; Frisch, H. L. *J. Appl. Phys.* **1967**, *38*, 2512.
26. Wang, C.; Liu, C. R. *Polymer* **1997**, *38*, 4715.
27. Chiu, F. C.; Yen, H. Z.; Lee, C. E. *Polym. Test.* **2010**, *29*, 397.
28. Wang, C.; Hwang, L. M. *J. Polym. Sci. Phys.* **1996**, *34*, 47.
29. Felix, J. M.; Gatenholm, P. *J. Mater. Sci.* **1994**, *39*, 3043.
30. Tomczak, F.; Satyanarayana, K. G.; Sydenstricker, T. H. D. *Compos. A Appl. S.* **2007**, *38*, 2227.
31. Tarrío-Saavedra, J.; López-Beceiro, J.; Naya, S.; Artiaga, R. *Polym. Degrad. Stabil.* **2008**, *93*, 2133.
32. Wang, Y.; Shi, J.; Han, L.; Xiang, F. M. *Mater. Sci. Eng. A Struct.* **2009**, *51*, 220.
33. Cong, P. H.; Xiang, F.; Liu, X. J.; Li, T. S. *Wear* **2008**, *265*, 1106.
34. Elghniji, K.; Soro, J.; Rossignol, S.; Ksibi, M. *J. Taiwan. Inst. Chem. E.* **2012**, *43*, 132.
35. Chiu, F. C.; Yen, H. Z.; Chen, C. C. *Polym. Test.* **2010**, *29*, 706.
36. Zhou, G. D.; Yao, Z.; Cao, K.; Li, B. G. *Polym. Mater. Sci. Eng.* **2009**, *25*, 101.
37. Zerbi, G.; Gallino, G.; Del Fanti, N.; Baini, L. *Polymer* **1989**, *30*, 2324.
38. Bagwasi, S.; Tian, B. Z.; Zhang, J. L.; Nasir, M. *Chem. Eng. J.* **2013**, *217*, 108.